お茶の水女子大学自然科学報告　第71巻　特別号
Natural Science Report, Ochanomizu University, Vol. 71, Special Issue（2020）

Tunneling Picture for the Resistance Peak in the In-Plane Magnetic Field

Woun Kang

Department of Physics, Ewha Womans University, Seoul 03760, Korea
wkang@ewha.ac.kr

(Received May 17, 2020)

Abstract: We explained the long standing puzzle on the mechanism for the resistance peak which appears when the magnetic field is precisely aligned along the conducting planes of layered materials. Using experimentally determined Fermi surface morphology in the layer, we showed that the interlayer conduction in the presence of strictly in-plane magnetic field is primarily governed by tunneling between two Fermi surfaces of adjacent layers. We successfully explained the azimuthal and field dependence of the peak resistance without invoking coherence of interlayer transport. So-called coherence peak results from a crossover between coherent and incoherent transport.

1. Introduction

Low dimensional layered materials have been intensively studied both for fundamental scientific interests and for the perspective of applications. One of the important problems in this class of materials is to understand the electronic transport properties between layers. Angle dependent magnetoresistance oscillations (AMRO) for various configurations of magnetic field rotation are particularly sensitive to the nature of the interlayer coupling and have been extensively studied in organic conductors [1-8], cuprates [9], intercalated graphites [10], ruthenates [11], and topological insulators [12].

The so-called *coherence* peak is an additional feature to the AMRO which is observed in some layered materials when the magnetic field direction lies within a few degrees from the conducting layers [13,14]. It is usually observed as a small peak superposed on the large background magnetoresistance and has long been regarded as a decisive evidence for the coherent nature of the interlayer transport [15]. However, the mechanism for the coherence peak has not yet been settled. It is proposed to result from the formation of small closed orbits that arise on the side of the warped Fermi surface cylinder in the magnetic field nearly parallel to the conducting plane [14], but it could be described as well by taking into account the role of the self-crossing orbits around the inflection point of quasi-two-dimensional (Q2D) Fermi surface [16].

Both of the above models, being based on the Q2D nature of the Fermi surface, assert that the angular width of the peak begins must be independent of temperature and magnetic field [14]. Surprisingly, our study shows that the width of the coherence peak strongly depends both on the magnetic field and on temperature. Therefore, it becomes very urgent to elucidate the underlying physics for the resistance peak.

Metallic state of β-(BEDT-TTF)$_2$I$_3$ under hydrostatic pressure higher than 1.5 kbar, has an exceptionally well defined Fermi surface [17-19] and showed extraordinarily well developed Shubnikov-de Haas oscillations [19], AMRO and the coherence peak (this work). We performed the detailed study of azimuthal, temperature and magnetic field dependence of the coherence peak using the organic layered conductor β-(BEDT-TTF)$_2$I$_3$. Unprecedentedly large peak height together with large AMRO dominates the magnetoresistance and allows us to study its temperature, field and azimuthal angle dependence

without paying much attention to the background behavior.

Temperature dependence of the peak resistance suggests an activated behavior and becomes saturated below 5 K. Tunneling model between two identical layers successfully explains both the azimuthal angle dependence and magnetic field dependence of the peak resistance. There is no need to invoke coherence of interlayer electron transfer to develop the resistance peak in the presence of only the in-plane magnetic field. So-called coherence peak results from a crossover from coherent to incoherent transport as the out-of-plane component of magnetic field vanishes.

2. Material and Methods

Conventional low-frequency ac technique is used for the interlayer resistance R_{zz} measurement, that is, the current is applied perpendicular to the plane of highly conducting layers and the voltage is measured between two outermost layers. Precise field alignment is crucial for this study because R_{zz} varies extremely rapidly within a few degrees from the conducting layer (θ = 90°). Moreover, the mounted sample position cannot be visually checked once the sample is embedded in a pressure cell. Our two-dimensional sample rotating system enables us to measure R_{zz} for all the 4π magnetic field directions from which we could find R_{zz} precisely at θ = 90° at any given ϕ direction.

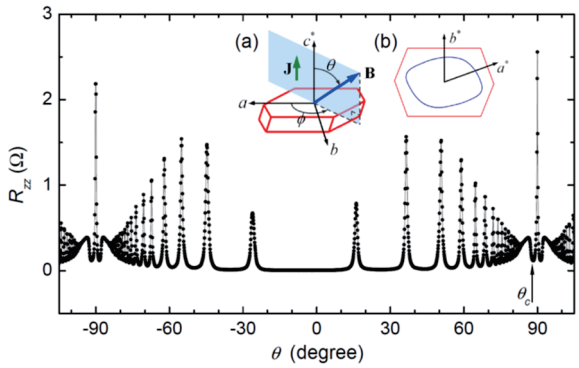

Figure 1. Typical angular dependence of R_{zz} of β-(BEDT-TTF)$_2$I$_3$ when the magnetic field rotates in a plane containing the axis normal to the conducting plane. More than 50 resonance peaks can be resolved in each side. Around $\theta = \pm 90°$, a pronounced peak appears accompanied with dips at both sides. $\phi \cong$ 158°, P = 7 kbar, B = 14 T and T = 1.5 K. R_{zz} at B = 0 is 4.64 x10^{-3}Ω. Insets: (a) Schematic diagram of β-(BEDT-TTF)$_2$I$_3$ crystal with crystallographic axis and definition of angles. z-direction is parallel to the c^*-axis. (b) First Brillouin zone (red line) based on the room temperature crystallography data [20] and the experimentally constructed Fermi surface (blue trace). Arrows are for directions only.

3. Results and discussion

Figure 1(a) shows the typical AMRO data when the magnetic field rotates in a plane containing the z-axis. There are more than 50 resonance peaks in each side which can be interpreted as the Yamaji oscillations [21]. They can be understood as an Aharanov-Bohm interference of tunneling between the Fermi surfaces of the adjacent layers shifted relative to each other by the in-plane component of the magnetic field [22]. Angles for the resonance peaks satisfy the well-known expression [21]

$$ck_F \tan\theta = \pi(n - \gamma)$$

where c is the spacing between neighboring conducting planes, k_F the Fermi wave vector at a given ϕ, n integer, and γ a phase factor smaller than 1. k_F can be obtained from plots of $\tan\theta$ at peak angles of magnetoresistance versus n. Projection of the Fermi surface to the layer was constructed from k_F values for 36 ϕ's after the standard procedure [23], and shown in Fig. 1(b) as a blue trace.

The background resistance monotonically increases until θ reaches within 3-4° to $\pm 90°$. But, beyond that characteristic angle, it develops a pronounced dip at θ_c (Fig. 1) before increasing sharply as θ further approaches $\pm 90°$. The interlayer magnetoresistance reaches up to about 55000% at 2 K for the field of 14 T along a direction in the layer, which

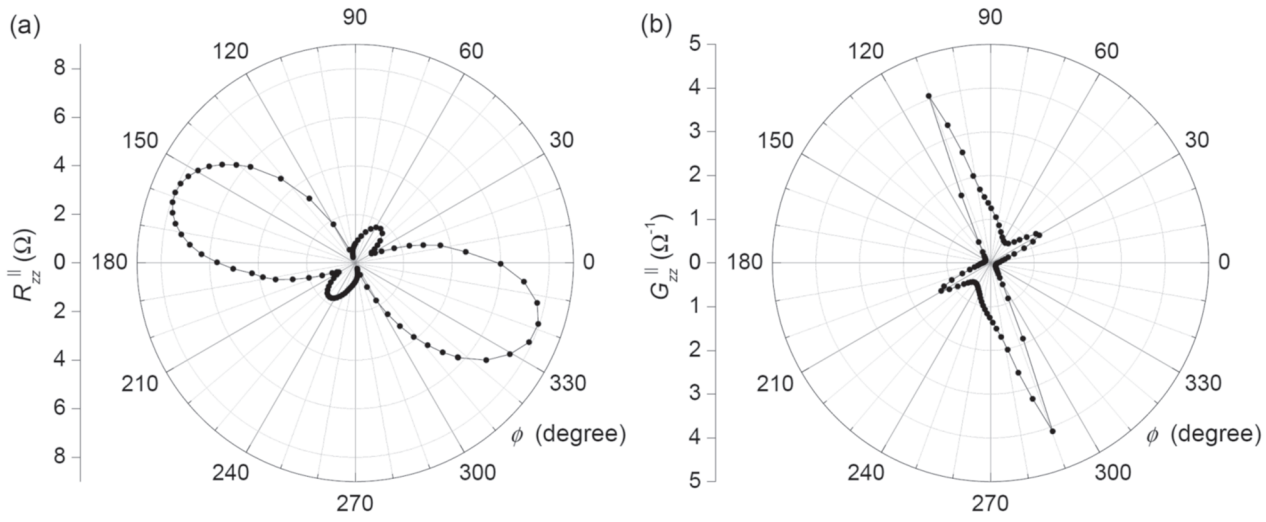

Figure 2. Azimuthal dependence of (a) interlayer resistance $R_{zz}^{\parallel}$ and (b) interlayer conductance $G_{zz}^{\parallel}$ at $\theta = 90°$. P = 11 kbar, B = 14 T and T = 1.5 K.

is extremely large for a nonmagnetic material [24]. Occurrence of the dip is related with the electron orbits near the inflection point of the Q2D Fermi surface, where the so-called self-crossing orbits begin to build around the belly. Logarithmically diverging cyclotron period for these orbits makes their average velocity along the *z* direction significantly large [16]. So, it has been proposed to be a good way to estimate the interlayer transfer integral t_c through the following relation [14].

$$\pi/2 - \theta_c = 2m^* t_c c/\hbar k_F$$

The resistance peak at $\theta = \pm 90°$ is of particular interest in this study. We used the symbol $R_{zz}^{\parallel}$ to denote the peak resistance at $\theta = \pm 90°$. Azimuthal dependence of $R_{zz}^{\parallel}$ and $G_{zz}^{\parallel}$ (= $1/R_{zz}^{\parallel}$) of the peak is shown in Fig. 2(a) and (b), respectively. $R_{zz}^{\parallel}(\phi)$ shows a two-fold rotational symmetry and consists of two kinds of lobes, one of which is much larger than the other. It is also worth of noting that except the conductance peak at 110° corresponding to the crystalline *b* direction, no other feature corresponds with any direct or reciprocal lattice vector or a combination of them.

There has been proposed either the closed orbits on the side of the warped cylindrical Fermi surface [14] or the open orbits nearly parallel to the cylinder axis of the Fermi surface [1,16,23] are responsible for the spectacular increase of resistance at $\theta = \pm 90°$. However, none of them could explain the azimuthal dependence of $R_{zz}^{\parallel}$, nor its temperature and magnetic field dependence.

$R_{zz}^{\parallel}$ under high magnetic field has unusual temperature dependence. Fig. 3 shows temperature dependence of $R_{zz}^{\parallel}$ for four different pressure values. Magnetic field direction is put along the maximum of $R_{zz}^{\parallel}$ in the conducting plane ($\phi \cong 158°$). Regardless of pressure values, there is a universal characteristics in the temperature dependence of $R_{zz}^{\parallel}$: (1) it is metallic above $T_{\min}$, (2) thermally activated between $T_{\min}$ and about 7 K ($T^{-1} \approx 0.14$ K^{-1}), and (3) becomes saturated below 3 K.

It is interesting to note that the activation energy divided by the Boltzmann constant Δ/k_B corresponds approximately the temperature where the resistance peak begins to emerge from the smoothly varying background around $\theta = 90°$. This suggests that the mechanism to produce sharp resistance peak at low temperature is tempered by the thermal energy and

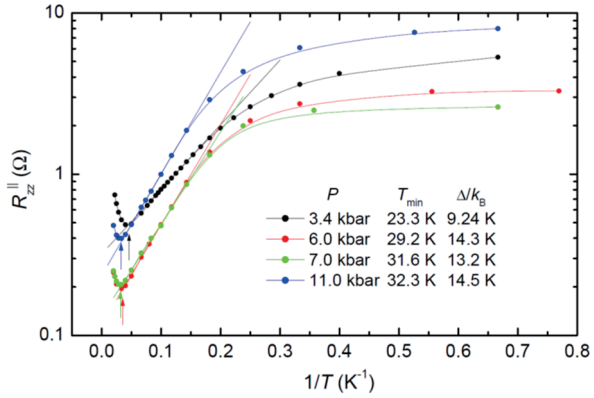

Figure 3. Temperature dependence of $R_{zz}^{\parallel}$ for four different pressure values. $R_{zz}^{\parallel}$ is metallic above $T_{\min}$ (upward arrows), activated between $T_{\min}$ and about 7 K, and saturated below 3 K. Activation energy is smaller at 3.4 kbar but saturates above 6 kbar.

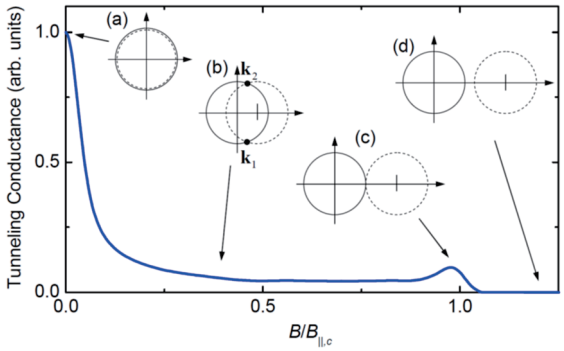

Figure 4. Magnetic field dependence of calculated tunneling conductance between two identical layers of free electrons. Insets depict relative alignment of Fermi surfaces for the upper layer (solid) and lower layer (dashed) for various field values: (a) $B_{\parallel} = 0$, (b) $0 < B_{\parallel} < B_{\parallel,c}$, (c) $B_{\parallel} = B_{\parallel,c}$, and (d) $B_{\parallel} > B_{\parallel,c}$. $B_{\parallel}$ is applied along upward in the paper and electrons tunnel from lower layer to upper one.

completely overwhelmed by thermally activated motion above the temperature of the order of the activation energy. Around 1.5 K where we performed most of azimuthal and field dependent measurements of $R_{zz}^{\parallel}$ the temperature effect can be safely ignored regardless of pressure value.

Here, we will show that the interlayer tunneling can explain the observed experimental results without invoking any semiclassical orbital motion of electrons. Let's consider a bilayer system consisted of two identical conducting layers separated by d. In the presence of magnetic field electron tunneling between two layers is described by the Hamiltonian [22]

$$\hat{H}_{\perp} = t_{\perp} \int \hat{\psi}_a^{\dagger}(\boldsymbol{r}) \hat{\psi}_b(\boldsymbol{r}) e^{ieA_z(\boldsymbol{r})d/\hbar} d^2r + H.C. \quad (1)$$

where the z-component of the vector potential is given by $A_z = B_{\parallel}x$. $t_{\perp}$ is the interlayer tunneling amplitude and $B_{\parallel}$ is the in-plane component of the magnetic field. Because of the gauge phase in Eq. (1), the in-plane electron momentum changes by $\Delta k_{\parallel} = eB_{\parallel}d/\hbar$ upon traveling between layers [22,25-27], so that the Fermi surfaces of the two layers are shifted relative to each other by $\Delta k_{\parallel}$ along perpendicular to the magnetic field. The tunneling current then becomes greatly reduced because electrons can tunnel only at the points where the conservation laws of both energy and momentum are satisfied [for example, the points $\boldsymbol{k}_a$ and $\boldsymbol{k}_b$ in Fig. 4 (b)].

Addition of perpendicular component of the magnetic field $B_{\perp}$ makes electrons do a cyclotron motion along the Fermi surface before tunneling through the points $\boldsymbol{k}_a$ and $\boldsymbol{k}_b$ although they are subject to a finite scattering time. Gauge phase is averaged over the entire Fermi surface during cyclotron motion and causes interference when there are several possible trajectories between two tunneling points. Ordinary AMRO could be successfully interpreted in this way [22].

On the other hand, there is no semiclassical cyclotron motion within layers when the magnetic field is strictly confined in the conducting layers. Only those electrons near the points $\boldsymbol{k}_a$ and $\boldsymbol{k}_b$ can tunnel from one layer to the other. This is a so stringent condition for electrons on the Fermi surface that the tunneling conductance falls sharply as soon as a magnetic field is

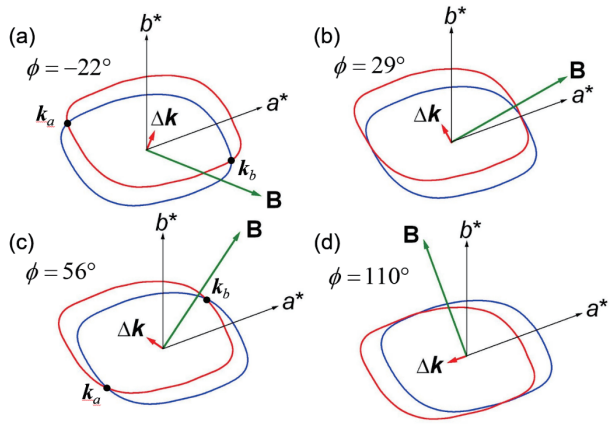

Figure 5. Fermi surfaces of two adjacent layers of β-(BEDT-TTF)$_2$I$_3$ for four different magnetic field directions within the layers. The Fermi surface of the upper layer (red) is displaced by $\boldsymbol{\Delta k_{\parallel}}$ along perpendicular to the magnetic field. The magnetic field directions $\boldsymbol{\phi = -22°}$ and $\boldsymbol{56°}$ correspond to those of maximal $\boldsymbol{R_{zz}^{\parallel}}$, and the directions $\boldsymbol{\phi = 29°}$ and $\boldsymbol{110°}$ to minimal $\boldsymbol{R_{zz}^{\parallel}}$, respectively. The size of $\boldsymbol{\Delta k_{\parallel}}$ in this figure is exaggerated by a factor of 30 for clarity.

applied (Fig. 4). Experiments for two purely two-dimensional electron layers in semiconductor structures confirmed the above model in which electron density in each layer could be controlled to keep the Fermi surface reasonably small so that the laboratory superconducting magnet could provide strong enough magnetic field $B_{\parallel,c} = 2\hbar k_F/ed$ to make the Fermi surfaces of two layers completely apart like in Fig. 4(d) [25].

However, when there is strong in-plane anisotropy with a significant distortion from the circular Fermi surface, the Fermi surfaces of neighboring layers share the same $\boldsymbol{k}$ over a broad section on the Fermi surface even after displacement along certain field directions. Fig. 5 shows the Fermi surfaces of two adjacent layers of β-(BEDT-TTF)$_2$I$_3$ when the magnetic field is applied along four different directions within layers. The size of $\boldsymbol{\Delta k_{\parallel}}$ in this figure is exaggerated by a factor of 30 for clarity.

Angles $\phi = -22°$ and $56°$ are directions where

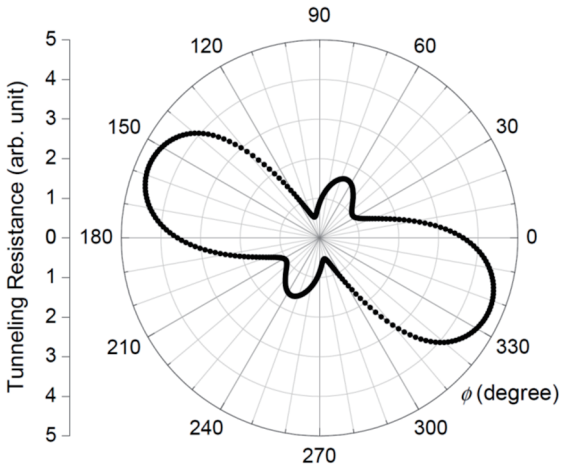

Figure 6. Azimuthal dependence of calculated interlayer resistance $R_{zz}^{\parallel}$ using Eq. 2 and the Fermi surfaces in Fig. 5

the peak resistance $R_{zz}^{\parallel}$ has primary and secondary maxima, respectively. It is evident that electrons can tunnel through only two points denoted with black dots. On the other hand, the Fermi surface has flat sections along $\Delta \boldsymbol{k}_{\parallel}$ at directions of $\phi = 29°$ and $110°$. Because all electrons on the flat area can tunnel from one layer to the other, interlayer conductivity develops sharp maximum for the field orientations around these angles. Because the situation in Fig. 5(a) or (c) prevails for most of ϕ values and the condition described in Fig. 5(b) or (d) is satisfied only over a narrow angular range, azimuthal dependence of $R_{zz}^{\parallel}$ must have broad maxima and sharp minima.

The tunneling current under the influence of small electric potential difference which is applied across the layers, can be represented by [25]

$$I_t \propto (R_{zz}^{\parallel})^{-1} \propto |M|^2 \int d^2\boldsymbol{k}_1 d^2\boldsymbol{k}_2 \times \delta(\varepsilon_1 - \varepsilon_{1,F})\delta(\varepsilon_1 - \varepsilon_2) f(\boldsymbol{k}_1 - \boldsymbol{k}_2) \qquad (2)$$

where ε_1 and ε_2 are electronic energies in the lower and upper layer, respectively. Similarly, $\boldsymbol{k}_1$ and $\boldsymbol{k}_2$ are wavevectors of electrons in the lower and upper layer, respectively. $\varepsilon_{1,F}$ is the Fermi energy of the lower layer and M is the tunneling matrix. The two δ

functions ensure that only those states near the Fermi energy contribute to the tunneling and that energy is conserved through tunneling. The f function contains the scattering information [25]. Fig. 6 shows the calculated interlayer resistance using Eq. (2) and the Fermi surfaces in Fig. 5. We assumed an isotropic Gaussian distribution of momentum transfers $f(q) \propto \exp(-q^2/2\Gamma^2)$ with $\Gamma = 0.05k_F$ and a constant tunneling matrix M over the Fermi surface. Considering the simplification that we used, agreement between experiment and calculation is excellent. Not only the shape of azimuthal dependence but also the relative magnitude is well reproduced. Sharper resistance dips in the measured data can be attributed to the detailed structure of the tunneling matrix M. It is remarkable that we do not need to invoke the coherent interlayer transport to understand the angular dependence of the so-called "coherence" peak.

Field dependence of tunneling conductance can also be calculated with Eq. (2) as in Fig. 4. The maximum displacement $\Delta \boldsymbol{k}_{\|}$ we can introduce to β-(BEDT-TTF)$_2$I$_3$ using the magnetic field of 14 T is at most ~3.2x10^7 m^{-1} which is two orders of magnitude smaller than the value to achieve the condition in Fig. 4(c). Therefore, we could observe only the beginning of the sharp decrease of tunneling conductivity with our available magnetic field.

Unusually sharp fall of the tunneling conductance signifies that the Fermi surface of the current system is very well and sharply defined as was already evidenced by exceptionally well developed Shubnikov-de Haas oscillations [19] and AMRO oscillations (Fig. 1). The falling curves of conductance for different field directions do not scale with $B_{\|,c}$. Instead, the falling rate is principally governed by the degree of superposition of the Fermi surfaces between two layers. The higher the conductance is on a given field direction, the slower the decreasing rate of conductance is. This observation strongly supports our tunneling model for the field and angle dependence of the resistance peak. The tunneling matrix M may vary significantly along the Fermi surface because of molecular nature of the current system, but our simple model cannot distinguish its influence.

4. Conclusion

We showed both experimentally and theoretically that the interlayer tunneling is a dominant mechanism for the sharp resistance peak which appears when the magnetic field lies parallel to the conducting layers. Contrary to the common belief, it is not necessary to invoke coherence of interlayer transport for its development. But, the dips on both sides of the resistance peak are still believed to be originated from the existence of the self-crossing orbits. Therefore, the so-called coherence peak results from a crossover between coherent and incoherent transport.

References

1. Kartsovnik, M. V., Kononovich, P. A., Laukhin, V. N., Schegolev, I. F., *Pis'ma Zh. Eksp. Teor. Fiz.* **48**, 498 (1988), [*JETP Lett.* **48**, 541 (1988)].
2. Kajita, K., Nishio, Y., Takahashi, T., Sasaki, W., Kato, R., Kobayashi, H., *Solid State Commun.* **70**, 1189 (1989).
3. Osada, T., Kawasumi, A., Kagoshima, S., Miura, N., Saito, G., *Phys. Rev. Lett.* **66**, 1525 (1991).
4. Naughton, M. J., Chung, O. H., Chaparala, M., Bu, X., Coppens, P., *Phys. Rev. Lett.* **67**, 3712 (1991).
5. Kang, W., Hannahs, S. T., Chaikin, P. M., *Phys. Rev. Lett.* **69**, 2827 (1992).
6. Osada, T., Kagoshima, S., and Miura, N., *Phys. Rev. Lett.* **77**, 5261 (1996).
7. Yoshino H., Murata, K., *J. Phys. Soc. Jpn.* **68**, 3027 (1999).
8. Kartsovnik, M. V., Chem. Rev. **104**, 5737 (2004).
9. Hussey, N. E., Abdel-Jawad, M., Carrington, A., Mackenzie, A. P., Balicas, L., *Nature* **425**, 814

(2003).
10. Enomoto, K., Uji, S., Yamaguchi, T., Terashima, T., Konoike, T., Nishimura, M., Enoki, T., Suzuki, M., Suzuki, I. S., *Phys. Rev.* B **73**, 045115 (2006).
11. Ohmichi, E., Adachi, H., Mori, Y., Maeno, Y., Ishiguro, T., Oguchi, T., *Phys. Rev.* B **59**, 7263 (1999).
12. Taskin, A. A., Segawa, K., Ando, Y., *Phys. Rev.* B **82**, 121302 (2010).
13. Danner, G. M., Kang, W., Chaikin, P. M., *Phys. Rev. Lett.* **72**, 3714 (1994).
14. Hanasaki, N., Kagoshima, S., Hasegawa, T., Osada, T., Miura, N., *Phys. Rev.* B **57**, 1336 (1998).
15. Moses P., McKenzie, R. H., *Phys. Rev.* B **60**, 7998 (1999).
16. Peschansky V. G., Kartsovnik, M. V., *Phys. Rev.* B **60**, 11207 (1999).
17. Murata, K., Tokumoto, M., Anzai, H., Bando, H., Saito, G., Kajimura, K., Ishiguro, T., *J. Phys. Soc. Jpn.* **54**, 2084 (1985).
18. Kang, W., Creuzet, G., Jerome, D., Lenoir, C., *J. Phys.* (Paris) **48**, 1035 (1987).
19. Kang, W., Montambaux, G., Cooper, J. R., Jerome, D., Batail, P., Lenoir, C., *Phys. Rev. Lett.* **62**, 2559 (1989).
20. Mori, T., Kobayashi, A., Sasaki, Y., Kobayashi, H., Saito, G., Inokuchi, H., *Chem. Lett.* **1984**, 957 (1984).
21. Yamaji, K., J. Phys. Soc. Jpn. **58**, 1520 (1989).
22. Yakovenko V. M., Cooper, B. K., *Physica* E **34**, 128 (2006).
23. Kartsovnik, M. V., Laukhin, V. N., Pesotskii, S. I., Schegolev, I. F., Yakovenko, V. M., *J. Phys.* I **2**, 89 (1992).
24. Takatsu, H., Ishikawa, J. J., Yonezawa, S., Yoshino, H., Shishidou, T., Oguchi, T., Murata, K., Maeno, Y., *Phys. Rev. Lett.* **111**, 056601 (2013).
25. Eisenstein, J. P., Gramila, T. J., Pfeiffer, L. N., West, K. W., *Phys. Rev.* B **44**, 6511 (1991).
26. Simmons, J. A., Lyo, S. K., Klem, J. F., Sherwin, M. E., Wendt, J. R., *Phys. Rev.* B **47**, 15741 (1993).
27. Boebinger, G. S., Passner, A., Pfeiffer, L. N., West, K. W., *Phys. Rev.* B **43**, 12673 (1991).

Acknowledgement

This work was supported by the National Research Foundation of Korea (NRF) grants funded by the Korean Government (MSIP) (2018R1D1A1B07050087, 2018R1A6A1A03025340). W.K. benefited from the visiting professorship of the ISSP, University of Tokyo.